Cellulose (2026) 33:4057–4075
https://doi.org/10.1007/s10570-026-07045-9

ORIGINAL RESEARCH

Nanocellulose-derived graphene quantum dots as bioenergy-enabling materials for dye-sensitized solar cells

Savisha Mahalingam · Abreeza Manap · Kam Sheng Lau · Chin Hua Chia · Nurfanizan Afandi · Faiz Arith · P Susthitha Menon · Nurul Atiqah Romli

Received: 20 April 2025 / Accepted: 13 April 2026 / Published online: 26 April 2026

Abstract Graphene quantum dots (GQDs) derived from nanocellulose were prepared with and without sulfuric acid pre-treatment, and applied in dye-sensitized solar cells (DSSCs). Using nanocellulose, a renewable carbon precursor from wood pulp, supports the development of bio-based materials for bioenergy and solar-to-electric energy conversion. Although acid treatment enhanced −COOH functionalization, excessive oxidation introduced structural defects that increased charge recombination and reduced photovoltaic performance. Acid-free GQDs produced higher photocurrent density than acid-treated samples, indicating better structural preservation and charge transport. However, both systems underperformed relative to conventional N719-only cells due to limited visible-light absorption and energy-level misalignment. Overall, acid-free synthesis offers a more sustainable route to nanocellulose-derived GQDs for environmentally friendly bioenergy and solar cell applications.

Keywords Co-sensitizer · Dye-sensitized solar cells · Energy · Graphene quantum dots

Introduction

The transition toward sustainable and low-carbon energy technologies has accelerated research on bioenergy-enabling materials—functional materials

S. Mahalingam (✉) · A. Manap (✉)
Institute of Sustainable Energy, Universiti Tenaga Nasional, Jalan IKRAM-UNITEN, 43000 Kajang, Selangor, Malaysia
e-mail: savisha@uniten.edu.my

A. Manap
e-mail: abreeza@uniten.edu.my

K. S. Lau (✉) · C. H. Chia
Materials Science Program, Department of Applied Physics, Faculty of Science and Technology, Universiti Kebangsaan Malaysia, 43600 Bangi, Selangor, Malaysia
e-mail: lauks@ukm.edu.my

N. Afandi
Department of Mechanical Engineering, College of Engineering, Universiti Tenaga Nasional, Jalan IKRAM-UNITEN, 43000 Kajang, Selangor, Malaysia

F. Arith
Faculty of Electronics and Computer Technology and Engineering, Universiti Teknikal Malaysia Melaka, Durian Tunggal, 76100 Hang Tuah Jaya, Melaka, Malaysia

P. S. Menon
Institute of Microengineering and Nanoelectronics, Universiti Kebangsaan Malaysia (UKM), 43600 Bangi, Selangor, Malaysia

N. A. Romli
Faculty of Computer and Mathematical Sciences, Universiti Teknologi MARA (UiTM) Perlis Branch, 02600 ArauPerlis, Malaysia

derived from biological resources that facilitate renewable energy generation and storage. Energy-related applications, such as supercapacitors, batteries, and solar cells, have attracted significant attention owing to the global demand for efficient and sustainable energy solutions (Mahalingam et al. 2016). Among these, dye-sensitized solar cells (DSSCs) have emerged as a promising alternative to traditional silicon-based photovoltaics due to their low production cost, environmental friendliness, and ease of fabrication (Abdullah et al. 2021). However, the efficiency of DSSCs is often limited by factors such as insufficient light absorption, charge recombination, and inefficient electron injection. To address these limitations, researchers have explored various strategies, including the incorporation of co-sensitizers (Onyemowo et al. 2024).

Co-sensitization involves the introduction of a secondary light-absorbing material in conjunction with the primary dye. This approach aims to broaden the spectral response of the device, improve light harvesting, and facilitate more efficient charge transfer (Li et al. 2014). Graphene quantum dots (GQDs) have attracted significant attention as potential co-sensitizers due to their tunable optical properties, high surface area, and excellent electron-transport capabilities (Mahalingam et al. 2021).

Quantum dot-sensitized solar cells have tunable bandgaps, high absorption coefficients, and the potential for multiple-exciton generation (Zeng et al. 2024). Chou et al. used green fluorescent GQDs (~ 530 nm) as a co-sensitizer with the N719 dye (Chou et al. 2023). The DSSC efficiency increased by 20%, primarily due to enhanced light absorption. In 2020, Jahantigh et al. synthesized nitrogen-doped GQDs with highly orange luminescence (~ 590 nm) and employed them, together with the N719 dye, as co-sensitizers in DSSCs (Jahantigh et al. 2020). They achieved a 40% increase in efficiency, which was attributed to enhanced light absorption. Mihalache et al. explained the dual role of co-sensitizers-GQDs as donors and acceptors for charge separation and collection, realizing a cascaded type-II alignment (Mihalache et al. 2015). However, the open-circuit voltage (V_{oc}) decreased by 30 mV compared to the conventional DSSC. This event can be attributed to GQDs' surface defects and trap states, which can trap electrons or facilitate recombination, thereby reducing Voc (Mihalache et al. 2015; Korir et al. 2024). Thus, surface modification of GQDs is essential.

Surface modification in GQDs enhances dispersion, improves charge transfer, and reduces recombination (John et al. 2021). GQDs tend to aggregate, which can hinder their performance. Surface modification can introduce functional groups that enhance their dispersion in solvents, resulting in a more uniform distribution within the DSSC (Saxena and Aswal 2015). Surface defects on GQDs can act as recombination centers (Rabeya et al. 2022). Surface modification can passivate these defects, thereby minimizing electron–hole recombination and enhancing photocurrent density (J_{sc}) and V_{oc} (Fu et al. 2020). Common surface modification techniques include functionalization with organic molecules (Qian et al. 2013), polymer coating (Gong et al. 2025), elemental doping (Mahalingam et al. 2025), acid or base treatment (Mahalingam et al. 2023), and plasma treatment (Yeh et al. 2024). Acids, particularly strong oxidizing acids such as nitric acid and sulfuric acid (H_2SO_4), can introduce oxygen-containing functional groups (carboxyl, hydroxy, epoxy) onto the GQDs' surface (Mahalingam et al. 2021). These functional groups enhance the hydrophilicity and dispersibility of GQDs in polar solvents. Acid treatment can also break down larger carbon structures into smaller GQDs, thereby enabling some degree of size control (Rasheed et al. 2024). However, acids such as hydrochloric acid and H2SO4 can cause severe oxidation, potentially damaging the GQDs' structure and reducing their conductivity (Bae et al. 2024).

H_2SO_4, due to its strong oxidizing nature, can etch the GQDs' surface, leading to vacancies, edge defects, and structural disorder (Hu 2022; Rabeya et al. 2022; Manjubaashini et al. 2024). Missing carbon atoms create holes in the GQDs lattice. Edge defects introduce functional groups at the edges of GQDs. Rabeya et al. reported that structural disorder in GQDs disrupts the sp2 carbon network and alters their electronic properties, including conductivity and charge-transfer behavior (Rabeya et al. 2022). They also noted that the etching process can increase surface area, which may be beneficial or detrimental depending on the specific application and degree of oxidation. Notably, in this study, the GQDs were derived from nanocellulose, a sustainable and abundant biomaterial. Unlike previous co-sensitization studies that used doped (Jahantigh et al. 2020) or plasma-treated

(Yeh et al. 2024) GQDs to enhance DSSC efficiency, this work investigates the impact of acid-free versus acid-treated synthesis pathways on GQDs derived from nanocellulose. Most prior studies focused on maximizing functionalization (e.g., via nitrogen doping) (Jahantigh et al. 2020) to improve charge transfer, but did not examine how excessive oxidation may degrade performance. The current work's findings reveal that while acid treatment enhances surface –COOH groups, it also introduces structural defects that reduce charge mobility and increase recombination. This nuanced trade-off has not been documented in prior reports, suggesting that moderate functionalization, rather than aggressive oxidation, may be more beneficial for GQD-based co-sensitizers.

Among renewable precursors, nanocellulose offers a sustainable pathway to produce carbon nanostructures owing to its high carbon content, nanoscale crystallinity, and abundance from wood pulp. Using nanocellulose as a carbon source not only reduces reliance on fossil-derived graphitic materials but also directly supports the bioenergy framework by valorizing biogenic feedstocks. Nanocellulose, extracted from plants, exhibits remarkable properties, including a high surface area, excellent mechanical strength, and biodegradability (Rahighi et al. 2021). These characteristics make it an attractive precursor for GQD synthesis. Utilizing nanocellulose as a starting material leverages its inherent advantages, contributing to a more environmentally friendly and sustainable approach to DSSC fabrication. The high surface area of nanocellulose, in particular, facilitates the efficient formation of GQDs with controlled size and morphology. Furthermore, the inherent functional groups in nanocellulose can facilitate surface modification of the resulting GQDs, thereby enhancing their interaction with the TiO_2 photoanode and the dye.

Despite increasing interest in biogenic carbons, the transformation of nanocellulose into graphene quantum dots and their implementation in dye-sensitized solar cells remain largely unexplored. This study bridges that gap by synthesizing nanocellulose-derived GQDs and demonstrating their potential as bioenergy-enabling materials for efficient solar-to-electric energy conversion. This work extends beyond a simple material comparison by demonstrating how the sustainable, acid-free synthesis of nanocellulose-derived GQDs affects not only surface chemistry but also the underlying electronic structure, which is critical for solar cell operation. Through systematic characterization, we demonstrate that strong-acid oxidation introduces trap states and shifts the lowest unoccupied molecular orbital (LUMO) level, thereby impairing electron injection into TiO_2. In contrast, acid-free GQDs exhibit more favorable energy alignment and reduced recombination losses. These findings highlight the importance of tuning both surface functionalization and electronic levels to optimize charge dynamics in GQDs-based DSSCs and support the use of green synthesis pathways for advancing next-generation photovoltaic materials.

The hypothesis is that acid treatment would enhance –COOH functionalization, improving dispersion and interfacial charge transfer, but might also introduce structural defects that promote recombination. The findings confirmed this trade-off: as functionalization increased, defect-induced recombination dominated, reducing DSSC performance. This work emphasizes the importance of balancing functionalization and structural integrity in GQD synthesis to achieve optimal solar cell efficiency.

Methodology

Materials

The nanocellulose used in this work was purchased from CelluForce (Canada). Nanocrystalline cellulose (NCC) is extracted from wood pulp obtained from PEFC-certified sources. According to CelluForce, its purity is 80–100 wt.% and contains up to 6% moisture depending on the environment (cellulose is hygroscopic and will adsorb moisture from the atmosphere). It is prepared by acid hydrolysis, followed by neutralization, washing, and drying.

Synthesis of acid-free GQDs

8.33 mg of nanocellulose is dissolved in 10 mL of DI water. The mixture was then ultrasonicated for 10 min to form a homogeneous dispersion. The nanocellulose dispersion is transferred to a microwave-safe vessel. The dispersion is microwave-irradiated at 120 ℃ for 2h at 600 rpm. The microwave power setting is 100-120W, and the pressure is ~ 2.1 bar during heating. After microwave treatment, the solution is

centrifuged at 12,000 rpm for 15 min to separate the GQDs from the reaction mixture. The GQDs supernatant is filtered using a 0.22 µm poly (tetrafluoroethylene) membrane filter to remove larger particles or impurities. The collected, acid-free GQDs are purified and dialyzed in a 1000-Da dialysis bag.

Synthesis of acid-treated GQDs

8.33 mg of nanocellulose is added to 5 mL of DI water. Then, 5 mL of 30% H_2SO_4 is added to the nanocellulose mixture solution. Both mixtures were sonicated for 10 min to form a homogeneous dispersion. The nanocellulose dispersion is transferred to a microwave-safe vessel. The dispersion is microwave-irradiated at 120 ℃ for 1h at 600 rpm. The microwave power setting is 100-120W, and the pressure is ~ 2.1 bar during heating. The reaction time was shorter than that for acid-free GQDs because the reaction is slow in the absence of a catalyst (H_2SO4). Thus, acid-free GQDs and acid-treated GQDs consumed 2h and 1h, respectively, under microwave irradiation. After microwave treatment, the solution is centrifuged three times at 12,000 rpm for 15 min to separate the GQDs from the reaction mixture. The GQDs supernatant is filtered using a 0.22 µm poly (tetrafluoroethylene) membrane filter to remove any larger particles or impurities. The collected acid-treated GQDs are further purified and dialyzed in a 1000 DA dialysis bag.

Fabrication of GQDs-based DSSCs

The photoanode was prepared using commercial TiO_2 paste (Ti-Nanoxide T/SP; Solaronix S.A.; Switzerland). The TiO_2 paste was coated onto fluorine-doped tin oxide conductive glass using the doctor-blade technique to create an active area of 0.25 cm^2, and then annealed in a dry furnace at 300 °C for 30 min. The annealed TiO_2 photoanode was post-treated with $TiCl_4$. Simultaneously, the synthesized GQDs and N719 ruthenium dye (Ruthenizer 535-bisTBA; Solaronix S.A., Switzerland) were mixed using a magnetic stirrer for 30 min on a hot plate (Mahalingam et al. 2022). Subsequently, the photoanodes were immersed in a GQDs + N719 mixture for 24h at 60 °C. The photoanode was then sandwiched between two FTO glass substrates, with platinum (Platisol-T; Solaronix S.A., Switzerland) used as the counter electrode. Both electrodes are separated by a Parafilm barrier, through which a drop-cast electrolyte (Iodolyte HI-30; Solaronix S.A., Switzerland) is deposited.

Characterizations

X-ray diffraction (XRD) (D8 Advance, Bruker AXS, Germany; 40 kV, 40 mA; Cu Kα1; Universiti Kebangsaan Malaysia, Malaysia) was used to identify the phase structure of nanocrystalline cellulose. XRD data were analyzed using Rietveld refinement via Materials Analysis Using Diffraction (MAUD) software (https://luttero.github.io/maud/). High-resolution transmission electron microscopy (HR-TEM) (JEM-2100F, 200 kV FE, JEOL; Universiti Putra Malaysia, Malaysia) was used to characterize the nanocellulose dispersion and the GQDs. The optical characterization was conducted using an ultraviolet–visible (UV–Vis) spectrometer (Perkin Elmer Lambda 35; Universiti Kebangsaan Malaysia, Malaysia) and a photoluminescence (PL) spectrometer (Perkin Elmer Lambda 35; Universiti Kebangsaan Malaysia, Malaysia). The structural properties of the samples were analyzed using a confocal Raman Microscopy system (Technospex uRaman-Ci; Nikon Eclipse Ci L laser microscope; Universiti Kebangsaan Malaysia, Malaysia). The chemical characterization was carried out using Fourier transform infrared spectroscopy (FTIR) (Agilent Technologies Cary 630; Universiti Kebangsaan Malaysia, Malaysia). The current density–voltage (J-V) characteristics (AutoLab) of the DSSC were measured under a standard illumination level of 100 mW/cm^2 using an AAA class solar simulator (ORIEL So13A, Newport; Universiti Tenaga Nasional, Malaysia). Multiple devices (five DSSCs per case) were prepared to ensure the reliability of the results. Electrochemical impedance spectroscopy (EIS) was used to study electron transport (Keithley instrument, Newport; Universiti Tenaga Nasional, Malaysia). The external quantum efficiency (EQE) was measured using a Bentham PVE300-IVT (Universiti Kebangsaan Malaysia, Malaysia). The density-functional theory (DFT) calculation for the GQDs was performed using Quantum Espresso, an open-source software package for electronic-structure calculations and nanoscale materials modeling. The

energy density is calculated using the generalised gradient approximation with the PBE functional, a cutoff frequency of 250 Ry, and a cutoff charge of 225 Ry.

Results and discussions

Nanocrystalline cellulose

The XRD diffractogram of NCC shows a semi-crystalline cellulose Iβ structure (Fig. 1). NCC was analyzed using Rietveld refinement in MAUD, and the fitted profile is shown in red. The refinement was based on the crystal structure of cellulose I reported by Nishiyama et al. (2002), and employed standard models suitable for anisotropic, fibrous cellulosic materials. The refinement proceeded in a stepwise manner to ensure stability and convergence.

A Chebyshev polynomial background function with 3 coefficients to environmental background correction from the blank XRD substrate holder. The phase scale factor (or incident beam intensity) is used to match the overall intensity level. Unit cell parameters are refined to [a = 7.735 Å, b = 8.346 Å, c = 10.172 Å, γ = 96.15°], remaining in close agreement with the starting values from Nishiyama et al. (2002). Preferred orientation using the March-Dollase model with the preferred axis along the {001} family of planes (c-axis direction). The March-Dollase coefficient (0.5) is consistent with the typical fiber-like alignment in cellulose materials that suppresses the intensity of the (004) reflection at 2θ ~ 34.5°. Profile broadening parameters: An initial isotropic crystallite size and microstrain were refined to provide a stable baseline fit. The final weighted profile R-factor (Rwp) was 2.93%, with a goodness-of-fit parameter of 1.887, indicating a satisfactory fit to the experimental data given the complexity of the microstructure and the presence of preferred orientation. The difference plot showed good agreement across the pattern, including reasonable modeling of the 004 peak after inclusion of the anisotropic size terms.

An explicit amorphous phase was tested by duplicating the cellulose I phase, binding structural and cell parameters, assigning a fixed isotropic crystallite size of 1.2 nm to model short-range disorder, and reducing the background polynomial to 1 coefficient. However, the amorphous scale factor was refined to effectively zero, with no meaningful improvement in Rwp or residuals compared to the crystalline-only model.

The d-spacing and crystallite size of (1–10), (110), (012), (200), and (004) planes were tabulated in Table 1 (Nishiyama et al. 2002; French 2014). The corresponding crystallite size distribution from 5.1 to 11.2 nm indicates heterogeneous domain sizes, which are common in acid-hydrolyzed NCC (Haouache et al. 2022; Park et al. 2010). The dramatic difference between planes reflects anisotropy in cellulose crystallites, with ordering along the chain axis (004) plane, which tends to produce larger coherent domains, whereas lateral planes show smaller sizes

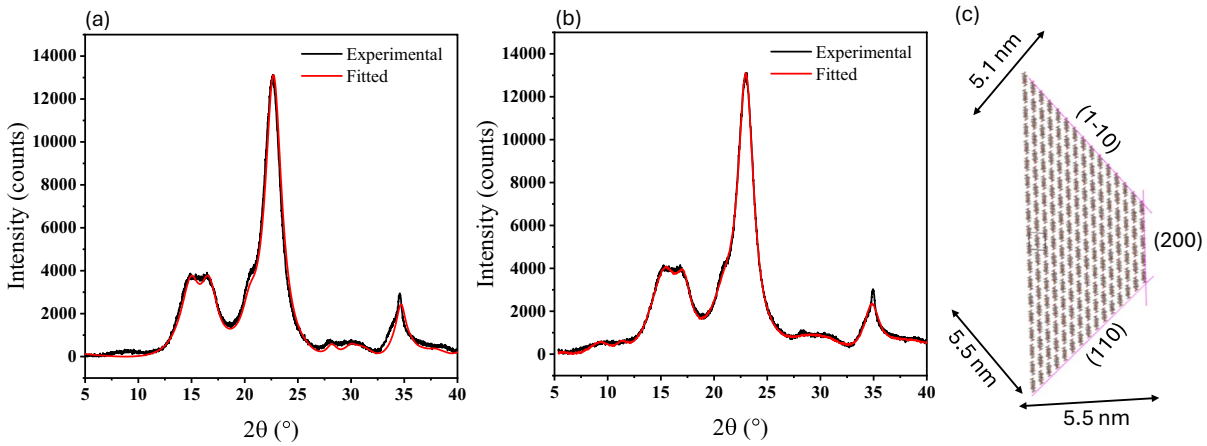

Fig. 1 X-ray diffraction spectra of nanocrystalline cellulose with **a** crystalline model, **b** amorphous model, and **c** graphical representation of the cellobiose unit cell crystal

Table 1 Crystallite size and d-spacing of nanocrystalline cellulose

2θ (°)	d-spacing (nm)	Plane (hkl)	Crystallite size (nm)
14.38	0.590	(1–10)	5.10
16.03	0.532	(110)	5.51
20.43	0.434	(012)	7.32
22.61	0.391	(200)	5.53
34.53	0.258	(004)	11.22

due to hydrolysis-induced fragmentation. The crystalline cellulose domains contribute to ordered carbon frameworks, while amorphous regions provide oxygen-rich functional groups that enhance luminescence properties (Jin et al. 2023).

Structure of nanocellulose dispersion

Figure 2 shows the HR-TEM images and SAED diffraction patterns of acid-free and acid-treated nanocellulose dispersions. The HRTEM micrographs clearly demonstrate the structural transformation induced by sulfuric acid hydrolysis. While the untreated nanocellulose exhibits highly bundled fibrous aggregates, typical of strong intermolecular hydrogen bonding, the acid-treated sample displays individual whisker-like nanocrystals with improved dispersion due to electrostatic repulsion from sulfate groups introduced during hydrolysis. This is because acid treatment can disrupt hydrogen bonding among nanocellulose fibers, resulting in a more dispersed structure (Niu et al. 2017).

Structure of graphene quantum dots

Figure 3 shows the HR-TEM images and SAED diffraction patterns of acid-free and acid-treated GQDs. The acid-free GQDs were still observed with some degree of aggregation, the same as in the dispersion form (Fig. 2a). Meanwhile, the acid-treated GQDs were separated individually. The absence of clumps indicates that the acid treatment effectively disrupts interparticle interactions, thereby improving GQD dispersion. This could be due to the introduction of hydrophilic functional groups (-OH, -COOH) during the acid treatment, which enhances the solubility and dispersibility of the GQDs.

Besides, acid-free GQDs are bigger (average size: 19.27 nm) than the acid-treated GQDs (average size: 13.64 nm). Although acid-free GQDs are bigger, all the quantum dots' sizes are almost similar (uniform particles). The acid-treated GQDs exhibit a size distribution of 6.59–19.21 nm (non-uniform particles). The larger average size of acid-free GQDs might be attributed to the absence of strong oxidizing agents that could effectively break down larger graphene structures into smaller GQDs. The broader size distribution of acid-treated ones indicates that the acid treatment has introduced a wider range of sizes. This could be due to the combined effects of structural

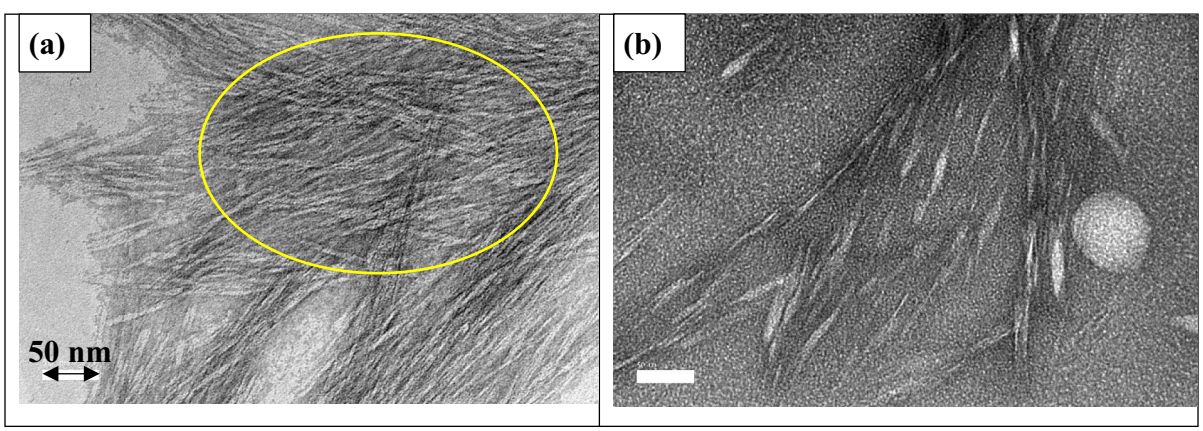

Fig. 2 HR-TEM images of **a** acid-free nanocellulose dispersion (aggregation is circled in yellow), and **b** acid-treated nanocellulose dispersion

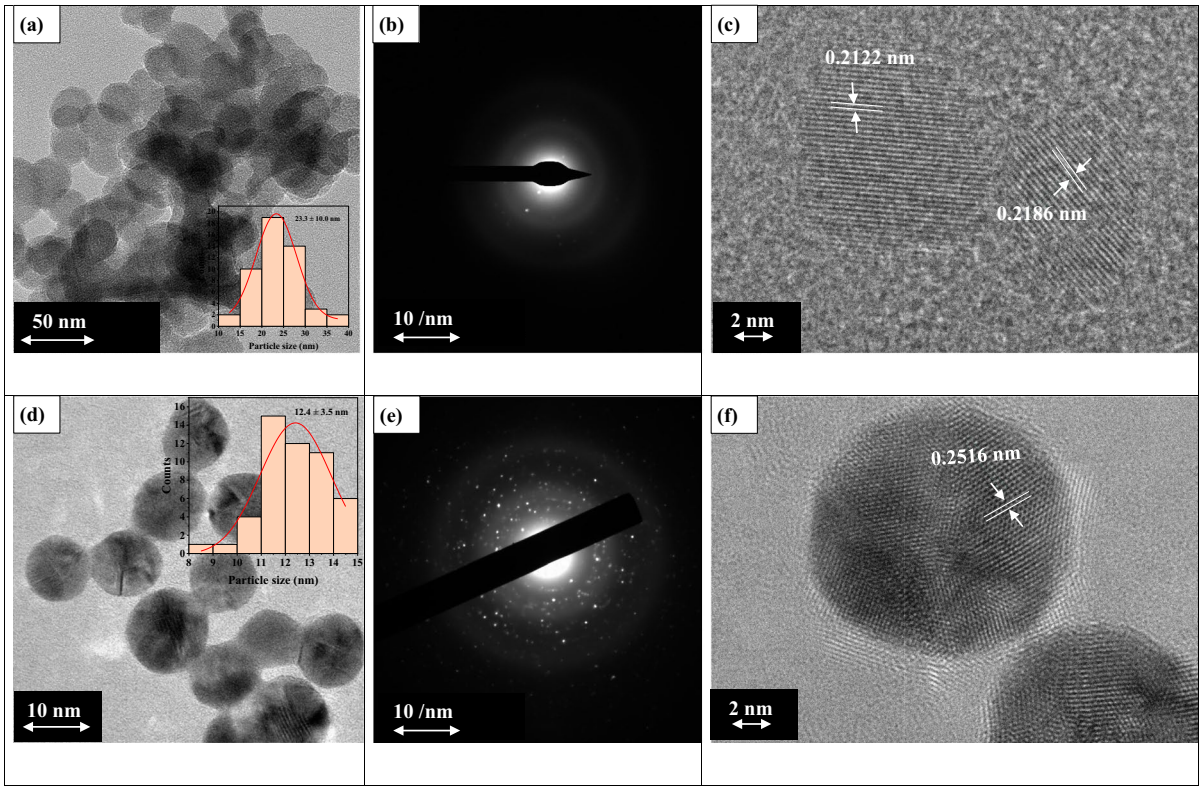

Fig. 3 Acid-free graphene quantum dots of **a** HR-TEM image, **b** SAED pattern, and **c** lattice fringe, and acid-treated graphene quantum dots of **d** HR-TEM image, **e** SAED pattern, and **f** lattice fringe

defects resulting from oxidative cleavage and edge effects. The edge defects in GQDs can be observed in Fig. 3c. Oxidative cleavage occurs when H_2SO_4 breaks down larger nanocellulose structures into smaller fragments, leading to a broader size distribution (Rabeya et al. 2022). The carbon edges are more reactive and can be further oxidized by the acid, resulting in larger, more irregular GQDs (Fig. 3c).

Furthermore, the SAED patterns indicate that both acid-free and acid-treated GQDs are polycrystalline, exhibiting ring-like diffraction patterns. However, the acid-GQDs have random white spots around the ring. Each white spot represents diffraction from a specific crystallite within the selected area. The random distribution of dots reflects the random orientation of these crystallites. The presence of defects (vacancies, grain boundaries) within the domains can also contribute to the diffuse scattering and the appearance of random dots. Acid treatment can introduce various defects into the GQD structure, including oxygen-containing functional groups, vacancies, and edge defects (Mahalingam et al. 2021). On the other hand, the acid-free GQDs, with distinct hexagonal dots on the ring, suggest the presence of small, ordered domains within the GQDs that exhibit a graphene-like hexagonal lattice.

Accordingly, each individual GQD belonging to acid-free has a single lattice fringe for acid-free and various lattice fringes for acid-treated ones. The acid-free GQDs exhibit lattice fringes of 0.2122 and 0.2186 nm, indicating more ordered, graphene-like structures. The acid-treated GQDs exhibit lattice fringes on a single quantum dot with lengths of 0.2516 nm, 0.2581 nm, 0.245 nm, and 0.2342 nm, indicating structural disorder or the presence of different crystallographic planes.

The lattice spacing of ~ 0.2 nm observed in both acid and acid-free GQDs corresponds to the (100) plane of the sp^2 carbon lattice within individual GQDs, rather than the interlayer spacing of stacked graphene sheets. This is consistent with previous reports on quantum-confined, single- or few-layer

GQDs, which typically exhibit in-plane atomic fringes of 0.21–0.24 nm. Li et al. (2012) reported a lattice spacing of ~ 0.21 nm for N-GQDs from HR-TEM, corresponding to the in-plane (100) lattice of graphitic carbon. This differs from the interlayer spacing of stacked graphene oxide or reduced graphene oxide sheets. For example, Akhavan (2010) reported an interlayer spacing of ~1 nm for graphene oxide due to oxygen-containing groups and ~0.34 nm for reduced graphene oxide after thermal reduction. In contrast, the GQDs obtained in this work are individual nanosized domains, and the ~ 0.2 nm spacing reflects their internal lattice periodicity rather than interlayer stacking. This distinction confirms the formation of crystalline GQDs rather than layered graphene oxide or reduced graphene oxide sheets.

XPS

Figure 4 shows the XPS spectra of acid-free and acid-treated GQDs. The high-resolution spectrum of C1s of acid-free (Fig. 4a) is deconvoluted into three surface components, corresponding to C=C (284.5 eV), C−O (286.2 eV), and C=O (288.2 eV). The strong peak at 284.5 eV corresponds to sp^2 hybridized carbon atoms (C=C bonds), indicating the graphitic nature of the GQDs (Eroglu and Metin 2023). On the other hand, acid-treated GQDs of C1s (Fig. 4c) were deconvoluted into four surface components, including C−C (285.0 eV), C−OH (285.7 eV), C−O (287.1 eV), and O=C−OH (289.2 eV). Following the methodology of Akhavan et al. (2012), the C 1s XPS spectra quantify the −COOH functional groups (~ 289.0 eV).

The acid-treated GQDs exhibit a −COOH peak with ~ 10% relative area, comparable to values reported for chemically oxidized graphene oxide, whereas acid-free GQDs show negligible −COOH content (< 2%). This confirms that acid treatment induces substantial oxidation, which correlates with observed structural defects and performance degradation. The C−C bond represents sp^3 hybridized carbon atoms, which are more prevalent in disordered regions (Nganglumpoon et al. 2024). There were

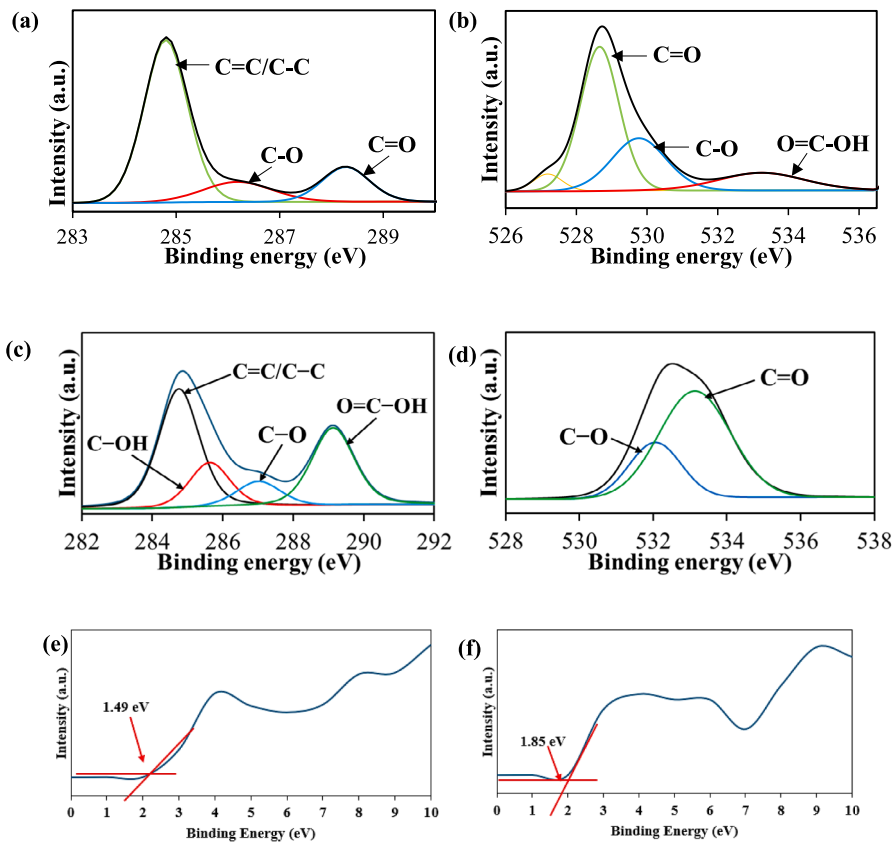

Fig. 4 XPS spectra of acid-free GQDs **a** C1s and **b** O1s, and acid-treated GQDs **c** C1s and **d** O1s, and band-gaps of **e** acid-free GQDs and **f** acid-treated GQDs

significantly enhanced peaks related to carbon–oxygen bonds (C−O, O=C−OH) at higher binding energies compared to acid-free GQDs. This demonstrates the successful introduction of oxygen-containing functional groups via acid treatment. These oxygen-containing groups disrupt the sp^2 network, contributing to the disorder.

The emergence of the −COOH group (285.7 eV), absent prior to treatment, demonstrates successful surface functionalization of the GQDs. They make the GQDs more hydrophilic, thereby improving their dispersibility in water (Hsiao and Lin 2020). Theoretically, −COOH groups in sensitizers are very useful for anchoring the dye to the TiO_2 electrode, promoting charge transfer (Zhang and Cole 2015). At the same time, it is possible that the −COOH group is associated with a defect site (Wang et al. 2016). The acid is reacting at defect sites and edge sites (Wang et al. 2016).

The high-resolution spectrum of O1s has a lower intensity in acid-free GQDs (Fig. 4b) than in acid (Fig. 4d) due to the lower oxygen content. There is an additional peak in acid-free GQDs, with a weak signal at 527.1 eV, corresponding to nanocellulose decomposition products that may be present on the GQDs' surface. This may create surface states that act as electron traps. A weak -COOH at 533.4 eV is observed for acid-free GQDs, and a dominant peak of -COOH is observed for acid-treated GQDs. This observation suggests that the acid-treated GQDs contain a high concentration of carboxyl groups. Moreover, the band gaps of GQDs were determined by the XPS survey spectrum (Guo et al. (2020), Hudait et al. (2013), Grządziel (2018) and found to be 1.49 eV and 1.85 eV for acid-free GQDs and acid-treated GQDs, respectively.

UV–Vis and PL

Figure 5 shows UV–Vis and PL spectra of acid-free and acid-treated GQDs. The acid treatment introduces oxygen-containing functional groups, such as carboxylic acids and hydroxy groups, onto the GQD surface, as observed in the XPS results (Fig. 5). These groups can significantly alter the electronic structure of the GQDs, leading to a shift of the absorption edge toward longer wavelengths (red shift) (Rani et al. 2023). However, the acid-treated GQDs exhibit only UV absorbance, suggesting that the acid treatment may have introduced defects or impurities that hinder visible-region absorption. Furthermore, the acid treatment process can sometimes alter the size and shape of GQDs. Smaller GQDs resulting from acid treatment tend to exhibit a blue-shifted absorption compared to larger ones due to quantum confinement effects (Li et al. 2013).

Meanwhile, acid-free GQDs likely retain a higher proportion of sp^2 carbon domains (aromatic structures) compared to acid-treated ones. These sp^2 domains contribute to the π-π* electronic transitions, which are responsible for the absorption in the visible region. The absence of acid treatment might result in fewer defects or impurities, leading to a more pristine GQD structure with better optical properties in the visible region.

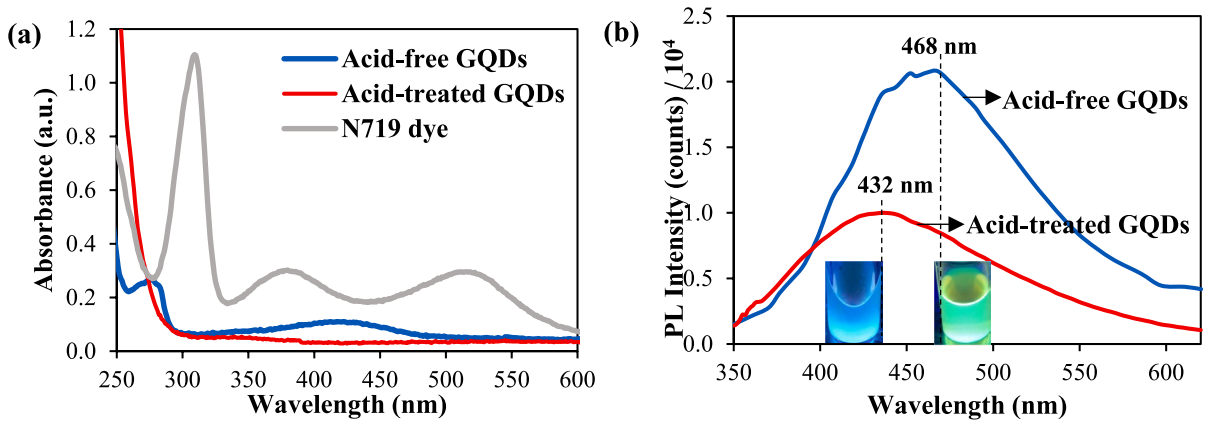

Fig. 5 **a** UV–Vis spectra, and **b** photoluminescence spectra of acid-free and acid-treated GQDs

Accordingly, the blue-shifted PL emission of acid-treated GQDs is likely due to a combination of strong quantum confinement effects (resulting from their smaller size) and the influence of surface functional groups and defects introduced during acid treatment. The smaller size of the acid-treated GQDs leads to stronger quantum confinement. This results in a more significant energy gap between the highest occupied molecular orbital and the LUMO. Thus, upon excitation, the electrons in acid-treated GQDs emit higher-energy photons, resulting in blue luminescence (λ = 432 nm). Acid treatment introduces oxygen-containing functional groups that can influence electronic transitions and emission properties.

The red-shifted PL emission of acid-free GQDs is primarily attributed to weaker quantum confinement effects (due to their larger size) and the electronic properties of the more pristine sp^2 carbon domains (Chen et al. 2020). Although the acid-treated GQDs exhibit a blue-shifted emission—typically associated with stronger confinement and smaller particle size—their PL intensity is significantly lower, likely due to non-radiative recombination pathways introduced by structural defects.

Raman and FTIR

Raman spectra of acid-free and acid-treated GQDs (Fig. 6 a) reveal distinct differences in structural disorder. The acid-treated GQDs exhibit a higher D band intensity and I_D/I_G ratio, indicating a greater degree of defect formation and lattice distortion due to strong oxidative treatment with H_2SO_4. This is consistent with our XPS and PL results, which show increased −COOH functionalization and the presence of non-radiative recombination centers. In contrast, the acid-free GQDs exhibit a lower I_D/I_G ratio, indicating fewer defects and improved retention of sp^2 carbon domains. Following the approach of Akhavan et al. (2015), who used Raman 2D band analysis to confirm graphene restoration after bioreduction, we note that our GQDs exhibit broad and weak 2D bands. The 2D band observed near ~ 2700/cm in both samples is broad and low in intensity, consistent with the presence of disordered, multilayered graphene domains typical of functionalized GQDs. The weak 2D feature in acid-free GQDs indicates limited graphitization. In

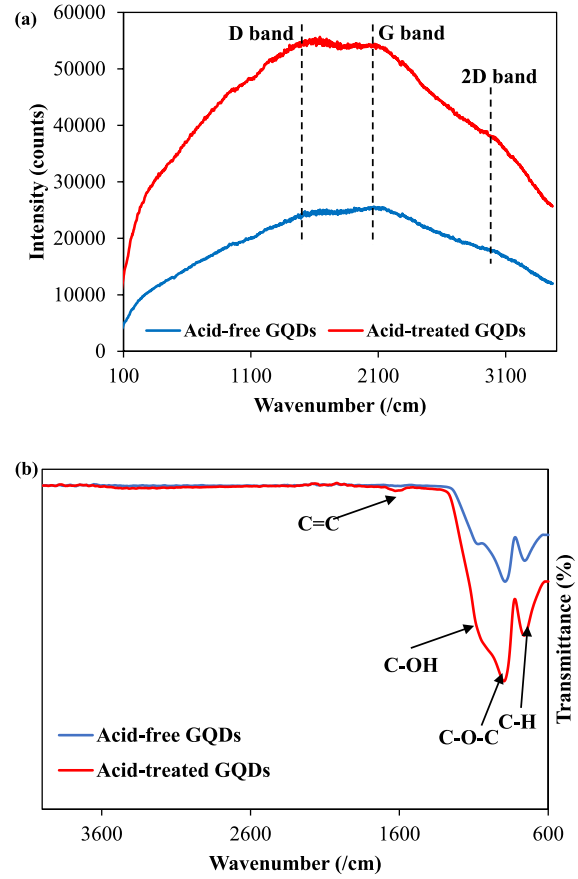

Fig. 6 **a** Raman and **b** FTIR spectra of acid-free and acid-treated GQDs

contrast, the broader 2D band in acid-treated GQDs reflects increased disorder from oxidation, supporting the non-crystalline nature of the synthesized dots.

FTIR analysis (Fig. 6 b) reveals that acid-treated GQDs exhibit stronger absorption bands corresponding to C−OH (~ 1400/cm), C−O−C (~ 1250/cm), and C−H (~ 1100/cm) vibrations, indicating extensive oxidation and the presence of oxygenated functional groups. In contrast, acid-free GQDs display a more pronounced C=C band at ~ 1600/cm, suggesting better preservation of sp^2 carbon domains. These findings confirm that acid treatment introduces significant structural disorder and surface oxidation, consistent with Raman and PL data, which collectively demonstrate that excessive oxidation degrades charge transport and photovoltaic performance.

Table 2 Quantum yield of acid-free and acid-treated GQDs

Quantum dots	Quantum yield (%)
Acid-free GQDs	5.22
Acid-treated GQDs	9.67

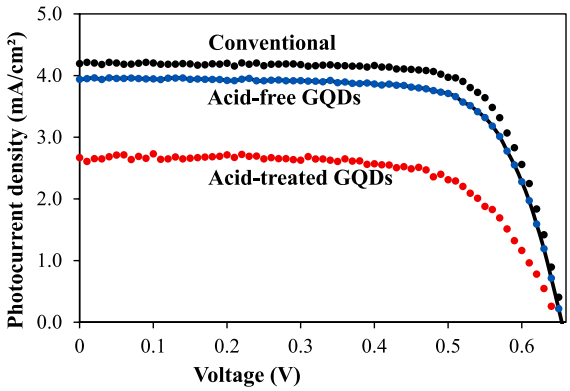

Fig. 7 J-V curves of conventional, acid-free, and acid-treated GQDs-based DSSCs

Quantum yield

Quantum yield (QY) is calculated using the following equation (Saafie et al. 2023).

$$QY = QY_R\left(\frac{I_S}{I_R}\right)\left(\frac{OD_S}{OD_S}\right)\left(\frac{\eta_S^2}{\eta_R^2}\right) \quad (1)$$

where S and R represent the sample of GQDs and R is the reference sample of quinine sulfate (0.1 M H_2SO_4; QY = 0.54; λ_{ex} = 350 nm). Meanwhile, I, OD, and η are the photoluminescence, absorbance value, and solvent's refractive index (Saafie et al. 2023).

Table 2 tabulates the resulting QY of acid-free and acid-treated GQDs. The acid-treated GQDs have a higher QY than the acid-free ones due to the presence of surface functional groups that can influence the electronic properties of GQDs, thereby affecting their radiative and non-radiative decay rates (Qian et al. 2013).

Current density–voltage analysis

Figure 7 demonstrates the J–V plots and the conforming photovoltaic parameters of conventional and GQDs-based DSSCs. Table 3 records the corresponding photovoltaic parameters. The V_{oc} remains nearly the same across all DSSCs, indicating that the introduction of GQDs did not alter it, whereas surface modification (acid treatment) improved it. Although the acid-free GQDs-based DSSC exhibited higher power conversion efficiency (η) than acid-treated ones, the η of both GQDs is still low compared to conventional DSSCs. In Fig. 7, the higher photocurrent density observed for acid-free GQDs is attributed to their lower degree of oxidation. Without harsh acid treatment, fewer defect states are introduced, minimizing electron trapping and recombination with the electrolyte or oxidized dye. This enables more efficient charge transport, leading to superior DSSC performance compared to acid-treated GQDs (Das et al. 2018). Meanwhile, acid-free GQDs have fewer defects, resulting in better performance than acid-treated GQDs. However, recombination might still be higher than in conventional DSSCs because co-sensitization introduces additional interfaces within the DSSC (Ashok Kumar et al. 2014). An EIS study was conducted to further investigate electron transport properties.

A significant change is observed in J_{sc}, where the conventional DSSC exhibits a higher J_{sc} than the acid-free GQDs. J_{sc} depends on how efficiently the dye (or co-sensitizers like GQDs) absorbs sunlight. Theoretically, co-sensitization of GQDs with N719 was supposed to broaden the solar absorption spectrum and boost the J_{sc} (Chou et al. 2023). However, in this study, the J_{sc} of GQDs-sensitization is lower than that of pure N719 dye sensitization. EQE was conducted to explore the reason for the low J_{sc}, as J_{sc} is

Table 3 J-V parameters of conventional, acid-free, and acid-treated GQDs-based DSSCs

DSSCs	J_{sc} (mA/cm^2)	V_{oc} (V)	FF	η (%)
Conventional	4.19 ± 0.02	0.67 ± 0.01	0.71 ± 0.001	1.98 ± 0.05
Acid-free GQDs	3.94 ± 0.005	0.65 ± 0.01	0.7 ± 0.01	1.79 ± 0.06
Acid-treated GQDs	2.67 ± 0.01	0.66 ± 0.01	0.65 ± 0.01	1.15 ± 0.03

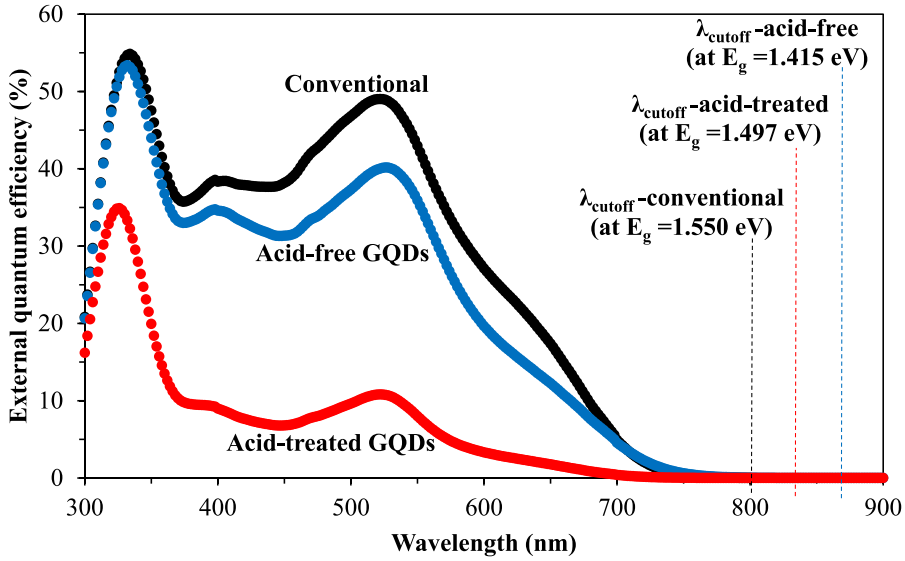

Fig. 8 External quantum efficiency of conventional, acid-free, and acid-treated GQDs-based DSSCs

directly proportional to the EQE spectrum integrated over the solar spectrum (Ananda 2017).

External quantum efficiency

Figure 8 demonstrates the EQE of conventional and GQDs-based DSSCs. The highest EQE was observed for the conventional case, following the same trend as η and J_{sc}. The cutoff wavelength (l_{cutoff}) is related to the bandgap energy (E_g) using the expression wavelength (nm) = 1240/energy (eV) (Huang et al. 2021). The E_g for N719 (800 nm), acid-free GQDs + N719 (876 nm), and acid-treated GQDs + N719 (828 nm) is 1.550 eV, 1.415 eV, and 1.497 eV, respectively. The extended absorption into the near-infrared (NIR) range by GQDs (at 876 nm for acid-free GQDs) may seem beneficial. However, NIR photons have lower energy and thus contribute less to the photocurrent. Additionally, solar intensity in the NIR region is significantly lower than in the visible range; therefore, extending the absorption into the NIR may not yield a substantial increase in J_{sc}. While GQDs absorb UV light and potentially extend absorption into the NIR region, their absorption cross-section is much smaller than that of N719. As a result, their contribution to the overall EQE and J_{sc} is minimal.

Additionally, GQDs typically have a smaller bandgap than N719. For example, the bandgap of acid-free GQDs is ~1.415 eV, while N719's bandgap corresponds to ~1.55 eV (as derived from the EQE cutoff wavelength of 800 nm). When GQDs are co-sensitized with N719, their absorption extends the light-harvesting range into the NIR region, effectively reducing the combined system's E_g. The EQE measures the overall efficiency of electron generation across the entire spectral range of light absorption. The introduction of GQDs shifts the EQE cutoff to longer wavelengths (lower energy), reflecting the minor bandgap contribution of GQDs.

Although acid-free GQDs and conventional DSSCs have similar EQEs in the UV region, the conventional DSSC has a higher EQE in the visible region. Co-sensitization can introduce additional recombination pathways due to the presence of multiple sensitizers with varying energy levels. Electrons injected by N719 or GQDs may recombine with holes before contributing to the photocurrent, reducing the EQE in the visible range. GQDs may create charge-trap states, further reducing electron transport efficiency in the visible range across the TiO_2 photoanode.

On the other hand, the acid-treated GQDs show low EQE even in the UV region. The acid treatment introduces oxygen-containing functional groups (−COOH, −OH) on the GQDs' surface, thereby creating trap states. These trap states may act as charge-recombination centers, reducing electron-injection efficiency into TiO_2 and lowering the overall contribution of absorbed UV light to the photocurrent.

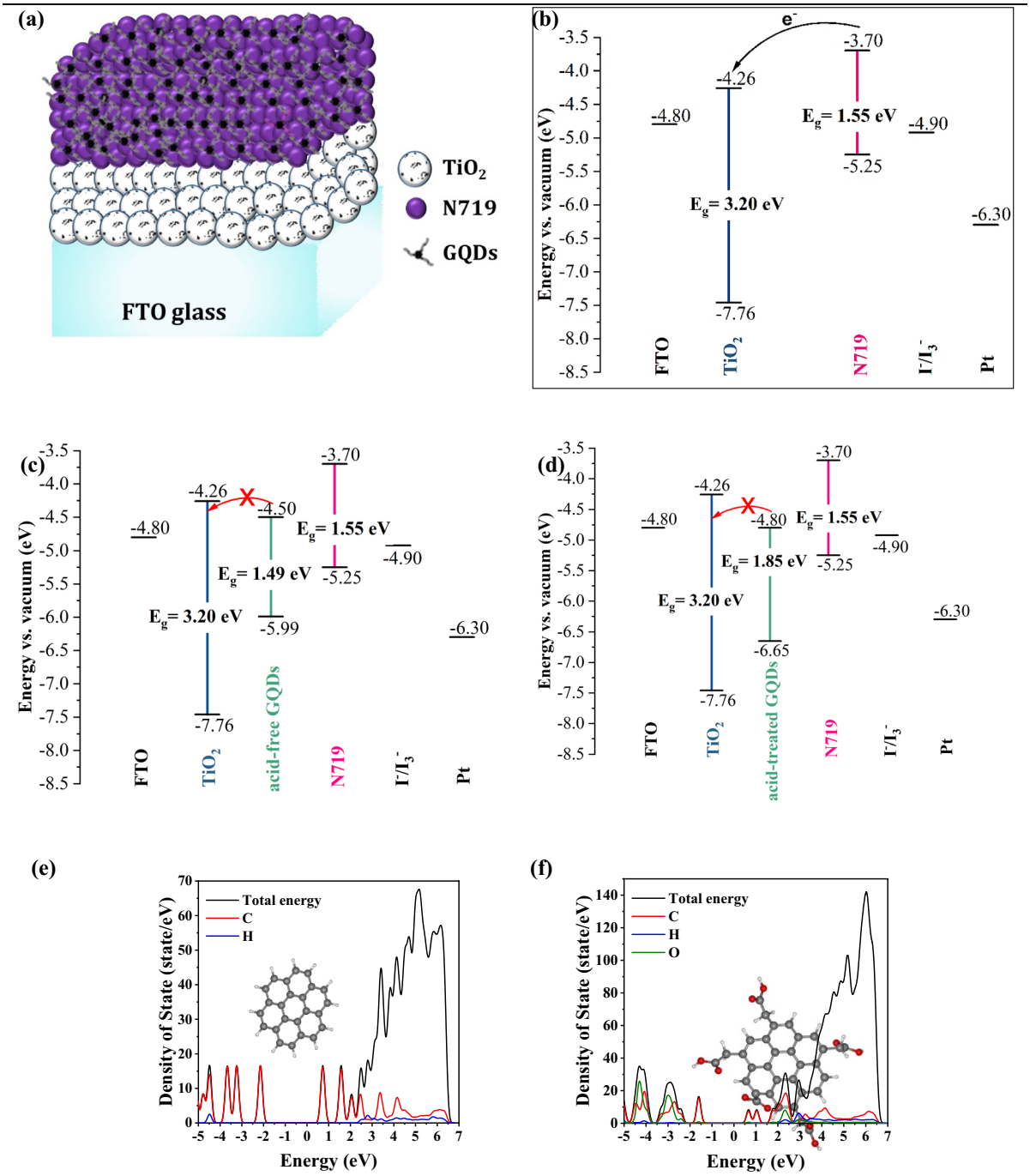

Fig. 9 **a** Schematic diagram of GQDs-based DSSC, energy band diagram of **b** conventional DSSC (TiO_2/N719), **c** TiO_2/acid-free GQDs + N719, **d** TiO_2/acid-treated GQDs + N719, and DFT of **e** acid-free GQDs, and **f** acid-treated GQDs

The UV region typically excites GQDs directly (as observed in the UV–Vis spectrum, Fig. 4), so low EQE in this region is often attributed to charge trapping and recombination. A detailed investigation will be analyzed in the EIS section.

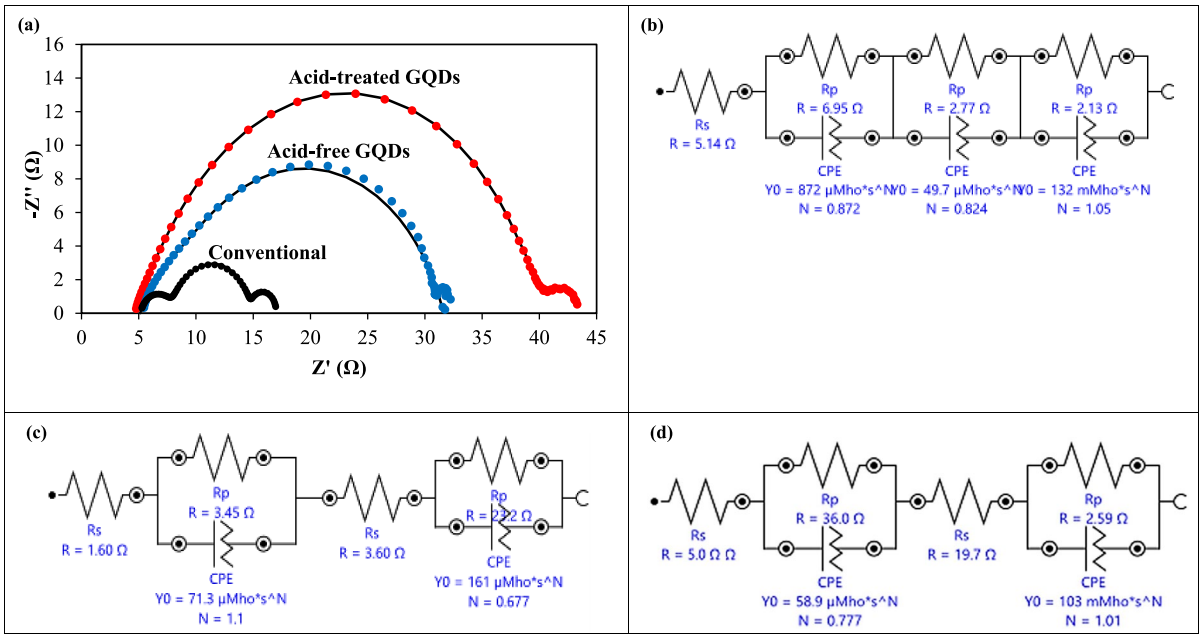

Fig. 10 **a** Nyquist and fitting spectra of DSSCs and corresponding equivalent circuit models of **b** conventional, **c** acid-free GQDs, and **d** acid-treated GQDs

Figure 9 shows the energy band diagram of conventional and GQDs-bsaed DSSCs. The conduction band of TiO_2 lies at approximately − 4.8 eV, while the excited state (LUMO) of N719 is at − 3.9 eV, allowing efficient electron injection into TiO_2. In contrast, GQDs synthesized in this study (band gaps determined by XPS) exhibit LUMO levels ranging from − 4.5 to − 6.65 eV, depending on size and surface state, which may be below the TiO_2 conduction band. This misalignment can hinder direct electron injection from N719 to GQDs. Furthermore, the highest occupied molecular orbital of GQDs is likely above the redox potential of the I^-/I_3^- electrolyte (~ − 4.9 eV), making regeneration inefficient. As a result, electrons excited in GQDs may recombine before injection or contribute weakly to current generation. This supports the observation of reduced J_{sc} and EQE in GQDs-based DSSCs compared to N719-only cells.

The density of states of acid-free and acid-treated GQDs is shown in Fig. 8d and e. The electron distribution in GQDs exhibits more electron delocalization due to the π-conjugation in the sp^2 carbon backbone structure. With the introduction of acid treatment, the GQDs will have a −COOH functional group on their surfaces, which can induce localized states from the non-bonding lone pairs of oxygen atoms and the π orbitals introduced by the −COOH groups. This causes the electron cloud to pull electron density towards O, creating localized electronic traps or states. The GQDs exhibit a delocalized π-electron distribution, which is optimal for charge transport and photoluminescence. Whereby GQDs–COOH reduce carrier mobility but enhance redox activity and surface reactivity, thereby tuning the bandgap and improving charge-transfer interactions.

Electron transport analysis

Figure 10 represents the Nyquist and fitted Nyquist plots of conventional, acid-free GQDs and acid-treated GQDs-based DSSCs. The corresponding equivalent circuit model is shown in the inset of Fig. 10. The EIS constraints are tabulated in Table 4. The electron lifetime (τ_n) and effective rate constant (k_{eff}) are determined using the following equations (Scarabino 2020).

$$\tau_n = \frac{1}{2\pi f_{max}} \quad (2)$$

$$k_{eff} = \frac{1}{\tau_n} \quad (3)$$

where, f_{max} is the maximum frequency of the Nyquist spectra,

Series resistance, $R_{s,}$ represents the ohmic resistance of the cell, including the contact resistance between the electrodes and the electrolyte resistance (Han et al. 2006). R_{ct} represents the resistance to charge transfer at the TiO_2/electrolyte interface (Ali et al. 2018). A lower R_{ct} indicates faster charge transfer and reduced recombination (Ali et al. 2018). Acid-free GQDs exhibit a significantly lower R_s value than conventional DSSC, indicating improved conductivity and reduced contact resistance. Acid-free GQDs, owing to their inherent properties, may enhance the conductivity of the TiO_2 film or facilitate better contact between the electrodes and the electrolyte. However, acid-free GQDs exhibit high Rct and a short electron lifetime, leading to increased recombination (k_{eff} = 7692.31/s) relative to conventional DSSCs. A higher R_{ct} indicates that charge transfer is hindered, meaning electrons are finding it more challenging to move from the TiO_2 to the electrolyte, or that recombination is increased (Kumar et al. 2017). Although acid-free synthesis may avoid some defects introduced by acid treatment, it can still introduce its own set of surface defects or structural imperfections, as evidenced by the XPS results. These defects can impede electron transfer from TiO_2 to the electrolyte. Moreover, the XPS results indicate that the acid-free GQDs exhibit surface chemistry that generates surface states that act as electron traps. These trapped electrons can then recombine with the electrolyte, increasing R_{ct}. This is evident in the HR-TEM image of the clumped dots of acid-free GQDs (Fig. 3a), which provides more sites for electron–hole recombination, leading to higher R_{ct} and a shorter electron lifetime.

Theoretically, functionalized GQDs with more -COOH groups may enhance the efficiency of GQDs (Mahalingam et al. 2021). However, in this work, we found that the R_{ct} is high for short τ_n in functionalized GQDs (acid-treated), thereby reducing the overall DSSC efficiency. Acid treatment, while introducing −COOH groups, can also introduce other defects into the GQDs' structure. The presence of too many −COOH groups can hinder electron transfer. They can create a dense layer of insulating groups that impede the movement of electrons (Martsinovich and Troisi 2011). The excess of −COOH groups could also disrupt the electron flow from the N719 dye (Martsinovich and Troisi 2011). Furthermore, acid treatment can alter the overall surface chemistry of the GQDs in ways that are detrimental to DSSC performance. As shown in the HR-TEM images, the acid-treated GQDs are well dispersed, while the acid-free GQDs are clumped. Even though the acid-free GQDs are clumped, this clumping is not as detrimental as the damage done to the GQDs by the acid treatment.

The conversion of renewable nanocellulose into conductive and photoluminescent GQDs highlights a sustainable route for fabricating active materials in solar devices. By coupling a bio-origin carbon source with an efficient photoelectrochemical process, this work advances the development of bioenergy-enabling materials that support the integration of green feedstocks into renewable energy technologies.

Conclusion

In summary, nanocellulose-derived graphene quantum dots were successfully synthesized and demonstrated effective performance in dye-sensitized solar cells. Beyond their optoelectronic function, the use of a renewable nanocellulose precursor underscores the role of bioenergy-enabling nanomaterials in bridging sustainable carbon sources with solar energy conversion, offering a pathway toward greener photovoltaic technologies. Although acid treatment was expected to enhance efficiency through increased −COOH functionalization, the results revealed the opposite. Most notably, the acid-treated GQDs, despite the anticipated increase in −COOH groups, exhibited the lowest DSSC efficiency. This was attributed to the introduction of significant defects during the acid treatment process, which drastically reduced τ_n and increased R_{ct}. This highlights that while −COOH functionalization is often associated with improved DSSC performance, excessive acid treatment can

Table 4 EIS parameters of conventional, acid-free, and acid-treated graphene quantum dots-based DSSCs

DSSCs	R_s (Ω)	R_{p1} (Ω)	R_{ct} (Ω)	R_{p3} (Ω)	C_{PE1} (Mho*s^N)	C_{PE2} (Mho*s^N)	C_{PE3} (Mho*s^N)	Kronig Kramers' test			f_{max} (Hz)	τ_n (ms)	K_{eff} (/s)
								X^2 (Z)	X^2 (Z')	X^2 (−Z'')			
Conventional	5.14	6.95	2.77	2.13	$Y_0 = 872e^{-6}$ N = 0.87	$Y_0 = 49.70e^{-6}$ N = 0.82	$Y_0 = 132e^{-3}$ N = 1.05	$2.23e^{-6}$	$5.49e^{-6}$	$1.68e^{-6}$	100	1.59	628.93
Acid free-GQDs	1.60	–	3.45	23.20	–	$Y_0 = 71.3\ e^{-6}$ N = 1.10	$Y_0 = 161e^{-6}$ N = 0.68	$11.60e^{-5}$	$2.16e^{-5}$	$9.41e^{-5}$	1258	0.13	7692.31
Acid treated-GQDs	5.00	–	36.00	2.59	–	$Y_0 = 58.90e^{-6}$ N = 0.78	$Y_o = 103e^{-3}$ N = 0.95	$3.77e^{-5}$	$1.52e^{-6}$	$2.25e^{-6}$	1995	0.08	12,500

have detrimental effects that outweigh the benefits of increased functional groups. Moreover, acid-free GQDs appear to enhance conductivity (low R_s) but simultaneously introduce pathways for increased charge recombination (high R_{ct}, short τ_n) compared with conventional DSSCs. The increased recombination outweighs the benefit of improved conductivity, resulting in lower overall efficiency. The GQDs may make better electrical contact with TiO_2, but they may also create more recombination sites. The findings of this study highlight the intricate relationship between GQD morphology, surface chemistry, and DSSC performance. Despite their lower oxidation state and reduced defect density, acid-free GQDs may be limited by aggregation because they lack polar functional groups. Incorporating appropriate surfactants or dispersion agents may mitigate this issue and improve photovoltaic performance. For future work, employing milder oxidants (e.g., dilute acids or organic acids) or controlling reaction time and temperature could offer a finer balance between surface functionalization and defect suppression.

Author contributions All authors contributed to the study conception and design. Material preparation, data collection and analysis were performed by Savisha Mahalingam and Kam Sheng Lau. The first draft of the manuscript was written by Savisha Mahalingam and Kam Sheng Lau and all authors commented on previous versions of the manuscript. All authors read and approved the final manuscript.

Funding This work was supported by Universiti Tenaga Nasional, Malaysia, through the AAIBE Chair of Renewable Energy, under the project codes of 202406KETTHA and J510051139.

Data availability The data that support the findings of this study are available from the corresponding author upon reasonable request.

Declarations

Conflict of interest The authors have no relevant financial or non-financial interests to disclose.

References

Abdullah H, Mahalingam S, Xian KJ, Manap A, Othman MH, Akhtaruzzaman M (2021) Impedance analysis of charge transfer upon nickel doping in TiO_2-based flexible dye-sensitized solar cell. Polym Bull 78(10):5755–5768

Akhavan O (2010) The effect of heat treatment on formation of graphene thin films from graphene oxide nanosheets. Carbon 48(2):509–519

Akhavan O (2015) Bacteriorhodopsin as a superior substitute for hydrazine in chemical reduction of single-layer graphene oxide sheets. Carbon 81:158–166

Akhavan O, Ghaderi E, Akhavan A (2012) Size-dependent genotoxicity of graphene nanoplatelets in human stem cells. Biomaterials 33(32):8017–8025

Ali AK, Ela SE, Hassoon KI et al (2018) Design of high-efficiency tandem dye-sensitized solar cell with two-photoanodes toward the broader light harvesting. Dig J Nanomater Biostruct 13:299–305

Ananda W (2017) External quantum efficiency measurement of solar cell. QiR 2017–2017 15th International Conference on Quality in Research (QiR): International Symposium on Electrical and Computer Engineering 2017-Dec:450–456. https://doi.org/10.1109/QIR.2017.8168528

Ashok Kumar K, Manonmani J, Senthilselvan J (2014) Effect on interfacial charge transfer resistance by hybrid co-sensitization in DSSC applications. J Mater Sci Mater Electron 25:5296–5301. https://doi.org/10.1007/s10854-014-2304-5

Bae G, Cho H, Hong BH (2024) A review on synthesis, properties, and biomedical applications of graphene quantum dots (GQDs). Nanotechnology 35:372001. https://doi.org/10.1088/1361-6528/ad55d0

Chen YX, Lu D, Wang GG et al (2020) Highly efficient orange emissive graphene quantum dots prepared by acid-free method for white LEDs. ACS Sustain Chem Eng 8:6657–6666. https://doi.org/10.1021/acssuschemeng.0c00106

Chou JC, Syu RH, Yang PH et al (2023) Graphene quantum dots as a co-sensitizer with improving light absorption for dye-sensitized solar cells. IEEE Trans Nanotechnol 22:20–27. https://doi.org/10.1109/TNANO.2023.3235335

Das TK, Ilaiyaraja P, Sudakar C (2018) Template assisted nanoporous TiO2 nanoparticles: The effect of oxygen vacancy defects on photovoltaic performance of DSSC and QDSSC. Sol Energy 159:920–929. https://doi.org/10.1016/j.solener.2017.11.061

Eroglu Z, Metin O (2023) Internal interactions within the complex type-II heterojunction of a graphitic carbon nitride/black phosphorus hybrid decorated with graphene quantum dots: implications for photooxidation performance. ACS Appl Nano Mater 6:7960–7974. https://doi.org/10.1021/acsanm.3c01187

French AD (2014) Idealized powder diffraction patterns for cellulose polymorphs. Cellulose 21(2):885–896

Fu L, Li H, Wang L et al (2020) Defect passivation strategies in perovskites for an enhanced photovoltaic performance. Energy Environ Sci 13:4017–4056

Gong C, Cui J, Sun Y et al (2025) Uniform electrodeposition of graphene/polypyrrole conductive coatings promoted by graphene quantum dots. Prog Org Coat 204:109269. https://doi.org/10.1016/j.porgcoat.2025.109269

Grządziel L, Krzywiecki M, Szwajca A, Sarfraz A, Genchev G, Erbe A (2018) Detection of intra-band gap defects states in spin-coated sol-gel SnOx nanolayers by photoelectron spectroscopies. J Phys D Appl Phys 51(31):315301 (**Jul 11;**)

Guo R, Zeng D, Xie Y, Ling Y, Zhou D, Jiang L, Jiao W, Zhao J, Li S (2020) Carbon nitride quantum dots (CNQDs)/TiO2 nanoparticle heterojunction photocatalysts for enhanced ultraviolet-visible-light-driven bisphenol A degradation and H2 production. Int J Hydrogen Energy 45(43):22534–22544 (**Sep 3;**)

Habibi Y, Lucia LA, Rojas OJ (2010) Cellulose nanocrystals: chemistry, self-assembly, and applications. Chem Rev 110(6):3479–3500 (**2010 Jun 9;**)

Hafid HS, Omar FN, Zhu J, Wakisaka M (2021) Enhanced crystallinity and thermal properties of cellulose from rice husk using acid hydrolysis treatment. Carbohydr Polym 260:117789. https://doi.org/10.1016/j.carbpol.2021.117789

Han L, Koide N, Chiba Y et al (2006) Modeling of an equivalent circuit for dye-sensitized solar cells: improvement of efficiency of dye-sensitized solar cells by reducing internal resistance. C R Chim 9:645–651. https://doi.org/10.1016/j.crci.2005.02.046

Haouache S, Jimenez-Saelices C, Cousin F, Falourd X, Pontoire B, Cahier K, Jérome F, Capron I (2022) Cellulose nanocrystals from native and mercerized cotton. Cellulose 29(3):1567–1581

Hsiao Y-J, Lin L-Y (2020) Enhanced surface area, graphene quantum dots, and functional groups for the simple acid-treated carbon fiber electrode of flexible fiber-type solid-state supercapacitors without active materials. ACS Sustain Chem Eng 8:2453–2461. https://doi.org/10.1021/acssuschemeng.9b06569

Hu Y (2022) From oxo-functionalized graphene to porous graphene and graphene quantum dots. Freie Universitaet Berlin, Germany

Huang G, Wang K, Markides CN (2021) Efficiency limits of c oncentrating spectral-splitting hybrid photovoltaic-thermal (PV-T) solar collectors and systems. Light Sci Appl. https://doi.org/10.1038/s41377-021-00465-1

Hudait MK, Zhu Y, Maurya D, Priya S, Patra PK, Ma AW, Aphale A, Macwan I (2013) Structural and band alignment properties of Al_2O_3 on epitaxial Ge grown on (100), (110), and (111) A GaAs substrates by molecular beam epitaxy. J Appl Physics. 113(13):134311

Jahantigh F, Ghorashi SMB, Mozaffari S (2020) Orange photoluminescent N-doped graphene quantum dots as an effective co-sensitizer for dye-sensitized solar cells. J Solid State Electrochem 24:883–889. https://doi.org/10.1007/s10008-020-04515-3

Jahantigh F, Ghorashi SB, Bayat A (2020) Hybrid dye sensitized solar cell based on single layer graphene quantum dots. Dyes Pigm 1(175):108118

Jin K, Song G, Diao H, Zhang X, Ji X, Zhang J, Zhang J (2023) Hydrogen-bond assisted nonconventional photoluminescence of crystalline and amorphous cellulose. Cellulose 30(13):8139–8150

John VL, Nair Y, Vinod TP (2021) Doping and surface modification of carbon quantum dots for enhanced functionalities and related applications. Part Part Syst Charact. https://doi.org/10.1002/ppsc.202100170

Korir BK, Kibet JK, Ngari SM (2024) A review on the current status of dye-sensitized solar cells: toward sustainable energy. Energy Sci Eng 12:3188–3226. https://doi.org/10.1002/ese3.1815

Kumar R, Nemala SS, Mallick S, Bhargava P (2017) High efficiency dye sensitized solar cell made by carbon derived from sucrose. Opt Mater (Amst) 64:401–405. https://doi.org/10.1016/j.optmat.2017.01.013

Li Y, Zhao Y, Cheng H, Hu Y, Shi G, Dai L, Qu L (2012) Nitrogen-doped graphene quantum dots with oxygen-rich functional groups. J Am Chem Soc 134(1):15–18

Li L, Wu G, Yang G et al (2013) Focusing on luminescent graphene quantum dots: current status and future perspectives. Nanoscale 5:4015–4039. https://doi.org/10.1039/c3nr33849e

Li H, Wu Y, Geng Z et al (2014) Co-sensitization of benzoxadiazole based D–A–π–A featured sensitizers: compensating light-harvesting and retarding charge recombination. J Mater Chem A 2:14649–14657. https://doi.org/10.1039/C4TA02777A

Mahalingam S, Abdullah H, Shaari S, Muchtar A (2016) Morphological and electron mobility studies in nanograss In_2O_3 DSSC incorporating multi-walled carbon nanotubes. Ionics 22(10):1985–1997

Mahalingam S, Manap A, Omar A et al (2021) Functionalized graphene quantum dots for dye-sensitized solar cell: key challenges, recent developments and future prospects. Renew Sustain Energy Rev 144:110999. https://doi.org/10.1016/j.rser.2021.110999

Mahalingam S, Manap A, Lau KS et al (2022) Mixture deposition method for graphene quantum dots-based dye-sensitized solar cell. Electrochim Acta 404:139732. https://doi.org/10.1016/j.electacta.2021.139732

Mahalingam S, Manap A, Rabeya R et al (2023) Electron transport of chemically treated graphene quantum dots-based dye-sensitized solar cells. Electrochim Acta 439:141667. https://doi.org/10.1016/j.electacta.2022.141667

Mahalingam S, Rabeya R, Manap A et al (2025) Electron transport in heteroatom-doped graphene quantum dots for TiO2-based dye-sensitized solar cells. Electrochim Acta 510:145369. https://doi.org/10.1016/j.electacta.2024.145369

Manjubaashini N, Daniel Thangadurai T, Nataraj D, Thomas S (2024) Graphene quantum dots: the emerging luminescent nanolights

Martsinovich N, Troisi A (2011) Theoretical studies of dye-sensitised solar cells: from electronic structure to elementary processes. Energy Environ Sci 4:4473–4495. https://doi.org/10.1039/c1ee01906f

Mihalache I, Radoi A, Mihaila M et al (2015) Charge and energy transfer interplay in hybrid sensitized solar cells mediated by graphene quantum dots. Electrochim Acta 153:306–315. https://doi.org/10.1016/j.electacta.2014.11.200

Nganglumpoon R, Poolboon K, Sitiputa P, et al (2024) Room-temperature synthesis and transformation of gqds from liquid oxygenates into nanocrystalline Sp2−Sp3 hybrid carbon. SSRN 4875628

Nishiyama Y, Langan P, Chanzy H (2002) Crystal structure and hydrogen-bonding system in cellulose Iβ from synchrotron X-ray and neutron fiber diffraction. J Am Chem Soc 124(31):9074–9082

Niu F, Li M, Huang Q et al (2017) The characteristic and dispersion stability of nanocellulose produced by mixed acid hydrolysis and ultrasonic assistance. Carbohydr Polym 165:197–204. https://doi.org/10.1016/j.carbpol.2017.02.048

Onyemowo M, Unpaprom Y, Ramaraj R (2024) Exploring the potential of natural dyes in DSSCs: innovations for efficient light harvesting and charge separation through co-sensitization. Opt Mater (Amst) 148:114860. https://doi.org/10.1016/j.optmat.2024.114860

Park S, Baker JO, Himmel ME, Parilla PA, Johnson DK (2010) Cellulose crystallinity index: measurement techniques and their impact on interpreting cellulase performance. Biotechnol Biofuels 3(1):10

Qian Z, Ma J, Shan X et al (2013) Surface functionalization of graphene quantum dots with small organic molecules from photoluminescence modulation to bioimaging applications: an experimental and theoretical investigation. RSC Adv 3:14571. https://doi.org/10.1039/c3ra42066c

Rabeya R, Mahalingam S, Manap A et al (2022) Structural defects in graphene quantum dots: a review. Int J Quantum Chem. https://doi.org/10.1002/qua.26900

Rahighi R, Panahi M, Akhavan O, Mansoorianfar M (2021) Pressure-engineered electrophoretic deposition for gentamicin loading within osteoblast-specific cellulose nanofiber scaffolds. Mater Chem Phys 1(272):125018

Rani P, Dalal R, Srivastava S (2023) Effect of surface modification on optical and electronic properties of graphene quantum dots. Appl Surf Sci. https://doi.org/10.1016/j.apsusc.2022.155379

Rasal AS, Korupalli C, Getachew G, Chou TH, Lee TY, Ghule AV, Chang JY (2021) Towards green, efficient and stable quantum-dot-sensitized solar cells through nature-inspired biopolymer modified electrolyte. Electrochim Acta 20(391):138972

Rasal AS, Lee TY, Kao PY, Gatechew G, Wibrianto A, Dirersa WB, Ghule AV, Chang JY (2022) Composition, morphology, and interface engineering of 3D cauliflower-like porous carbon-wrapped metal chalcogenides as advanced electrocatalysts for quantum dot-sensitized solar cells. Small 18(32):2202133

Rasal AS, Subrahmanya TM, Kizhepat S, Getachew G, Ghule AV, Devan RS, Hung WS, Fahmi MZ, Wibrianto A, Chang JY (2025) Carbon quantum dots: classification-structure-property-application relationship for biomedical and environment remediation. Coord Chem Rev 15(533):216510

Rasheed PA, Ankitha M, Pillai VK, Alwarappan S (2024) Graphene quantum dots for biosensing and bioimaging. RSC Adv 14:16001–16023. https://doi.org/10.1039/D4RA01431F

Saafie N, Sambudi NS, Wirzal MD, Sufian S (2023) Effect of hydrothermal conditions on Kenaf-Based carbon quantum dots properties and photocatalytic degradation. Separations 10(2):137

Saxena V, Aswal DK (2015) Surface modifications of photoanodes in dye sensitized solar cells: enhanced light harvesting and reduced recombination. Semicond Sci Technol 30:064005. https://doi.org/10.1088/0268-1242/30/6/064005

Scarabino S (2020) Mechanistic analysis of dye regeneration and mass transport processes at dye-sensitized solar cells using microelectrochemical experiments. Doctoral dissertation, Oldenburg, Universität Oldenburg

Wang S, Cole IS, Zhao D, Li Q (2016) The dual roles of functional groups in the photoluminescence of graphene quantum dots. Nanoscale 8:7449–7458. https://doi.org/10.1039/C5NR07042B

Yeh Y-J, Liou JR, Lin W et al (2024) Plasma-engineered GQD-inorganic membranes with tunable interactions for ultrahigh-efficiency molecular separations. J Membr Sci 690:122248. https://doi.org/10.1016/j.memsci.2023.122248

Zeng HH, Rasal AS, Abate MA, Ghule AV, Chang JY (2024) Surface and interfacial engineering for aqueous-processed quantum dots-sensitized solar cell with efficiency approaching 11%. Chem Eng J 1(495):153702

Zhang L, Cole JM (2015) Anchoring groups for dye-sensitized solar cells. ACS Appl Mater Interfaces 7:3427–3455. https://doi.org/10.1021/am507334m